Fusion Engineering and Design 193 (2023) 113805

Contents lists available at ScienceDirect

Fusion Engineering and Design

journal homepage: www.elsevier.com/locate/fusengdes

Integration of new sets of magnets for improved plasma confinement in the SPIDER experiment

N. Marconato [a,b,*], G. Berton [a], V. Candeloro [a,d], E. Sartori [a,c], B. Segalini [a,d], G. Serianni [a]

[a] Consorzio RFX, CNR, ENEA, INFN, Università di Padova, Acciaierie Venete SpA, Corso Stati Uniti 4, 35127 Padova, Italy
[b] Department of Industrial Engineering (DII), University of Padua, 35131 Padova, Italy
[c] Dept. of Engineering and Management, Univ. of Padova, Strad. S. Nicola 3, 36100, Vicenza, Italy
[d] Centro Ricerche Fusione (CRF) - UNIPD, Corso Stati Uniti 4, 35127 Padova (PD), Italy

ARTICLE INFO

Keywords:
NBI
Magnetic field
Permanent magnets
Magnetic shield
FEM
Plasma
RF drivers

ABSTRACT

SPIDER is the full-scale prototype of the plasma source of the negative-ion driven neutral beam injector for the heating and current drive of the ITER plasma. The uniqueness and complexity of the system requested this ad hoc test stand aiming at optimizing the performance of the RF inductively generated plasma, negative ion production and extraction, electron filtering, and robustness and controllability of all systems required to work together. After about three years of operation, presently SPIDER is in a long shutdown, in which the whole plasma source and accelerator were dismounted. In this phase, additional modifications with respect to the original design will be introduced to improve the system performance, driven by the experience acquired in the last years.

These include the addition of further sets of permanent magnets in the plasma source expansion chamber and around the RF drivers, with the aim of improving the plasma confinement and consequently its density and possibly its uniformity. The present paper reports the study and the analyses behind this modification, which impacts on the original already complex magnetic configuration, made particularly difficult by the limited space available and the high voltages. The use of ferromagnetic shields, necessary to limit stray fields possibly increasing the breakdown probability, make the design particularly complex because of the greater impact on the previous configuration. An iterative process between analyses to determine the ideal configuration and CAD verifications was required. The analyses had to take into account the new magnetic configuration to be created in the particular area of interest, and the overall configuration in order to not compromise its efficacy.

1. Introduction

ITER, the experimental nuclear fusion reactor presently under construction in Cadarache, France, is an international project aimed at demonstrating the feasibility of nuclear fusion as future clean and long lasting energy source. The main goals are filling the gap in the present understanding of burning plasma physics and the consequent achievement of a comprehensive control capability required to obtain and maintain plasma parameters necessary for significant fusion power production, together with the many technological challenges this entails. The high temperature of the plasma, required for a sufficient amount of fusion reactions to occur, and the need of long pulse duration call for additional heating and current drive systems with respect to the only inductively generated plasma current and related Joule heating. A combination of Electron Cyclotron Resonance Heating, Ion Cyclotron Resonance Heating and Neutral Beam Injectors (NBIs) is foreseen for the required auxiliary input power of about 50 MW [1]. Two NBIs are foreseen to supply a total power of 33 MW, by accelerating negative deuterium ions to 1 MeV [2]. A dedicated Neutral Beam Test Facility (NBTF) was set up at Consorzio RFX (Italy) in order to develop for the first time a system capable of achieving simultaneously the ITER NBI requirements [3]. NBTF includes two experiments. MITICA (Megavolt ITER Injector and Concept Advancement), presently under construction, is the full-scale prototype of the whole ITER NBI, where the 1 MV voltage holding issues will be studied together with the neutralization of the negative ion beam. SPIDER (Source for the Production of Ions of Deuterium Extracted from RF plasma) is the full-scale prototype of the ITER NBI source with 100 keV beam accelerator, with the aim of achieving the requirements in terms of negative ion current (40 A) for a beam-on time of 1 h [4]. In particular, SPIDER aims at optimizing the ion

* Corresponding author.
E-mail address: nicolo.marconato@igi.cnr.it (N. Marconato).

https://doi.org/10.1016/j.fusengdes.2023.113805
Received 27 October 2022; Received in revised form 29 April 2023; Accepted 9 May 2023
Available online 15 May 2023

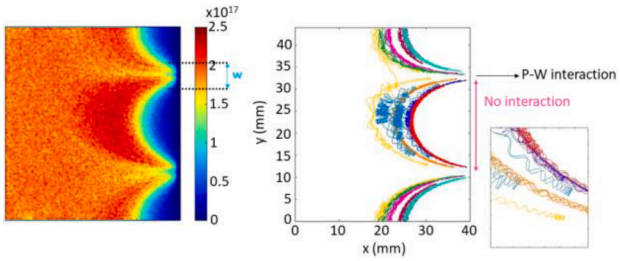

Fig. 1. Example of Particle-In-Cell simulation of plasma –wall interaction in the presence of two cusp magnets (periodicity is applied on top/bottom boundaries).

source performance in terms of uniformity of the source plasma and extracted current over a beam area of about 1.5 m^2, negative ion current density (355 A/m^2 in H^- and 285 A/m^2 in D^-) and beam optics, for continuous beam operation of 3600 s.

The present paper describes the review and integration of the magnetic configuration during the present long shutdown, which started at the end of 2021, with new sets of permanent magnets (PM) and magneto-static shields (MSS) in order to improve the plasma confinement in the SPIDER ion source, driven by the experience acquired in the last years. In Section 2 motivations of the modifications are explained; in Section 3 the new Driver magnet set is described; the new sets on the source case walls are described in Section 4; the overall magnetic field is considered in Section 5, with special concern to the uniformity of the field due the interplay among different sources; and finally conclusions are drawn in Section 6.

2. Motivations

Since the beginning of SPIDER operation in 2018, many issues have been solved, modification implemented, lessons learned and objectives reached. The influence of the magnetic field on the uniformity and overall performance of the system resulted to be of primary importance. In any negative ion driven NBI, the magnetic field is essential to reduce the electron temperature in the extraction region, in order to minimize the destruction rate of negative ions (the rate of electron detachment by electron impact decreases by a factor of 10 when the electron temperature decreases from 4 to 1 eV). It also minimizes the diffusion of electrons towards the extraction, so that in the presence of negative ions, the co-extracted electron current from the plasma can be minimized. In SPIDER this is realized by the Filter Field (FF) produced with a DC (or slowly varying) electric current (up to 5 kA) flowing in the plasma facing electrode (plasma grid, PG) and closing in an assembly of bus-bars specifically positioned. In addition, different sets of PMs embedded in components of both the ion source and the accelerator are present, so that a complex magnetic field configuration is produced. The integration of permanent magnets in the plasma source walls, with a cusp configuration, is a typical expedient to minimize the plasma loss by interaction with the wall [5]; multi-cusp configurations are commonly used in negative ion sources [6]. In general, plasma electrons are magnetized by the cusp field so that the plasma-wall interaction takes place on a limited width w in correspondence of the magnets, usually called leak width. Fig. 1 shows the effect of the magnetic field on the plasma (left) and single electron trajectories (right) in a periodic particle-in-cell simulation. The leak width, w, is also highlighted. The plasma density of 2×10^{17} m^{-3}, electron temperature of about 2 eV, and the B field strength at the wall of 120mT, are somewhat relevant to the case of the SPIDER lateral walls. In SPIDER, cusp magnets are integrated in the rear disk of the RF drivers, and embedded on the lateral wall of the plasma expansion chamber, the so called Source Case Later Wall (SCLW) where the FF lines cross the wall perpendicularly.

In 2020 the bus-bar arrangement was modified with respect to the original design [7] in order to improve the plasma confinement in the RF drivers, by changing the topology of the magnetic field and reducing its intensity inside the drivers, as described in [8]. The modification was found to be successful, in the sense that the plasma density inside the drivers was measured to monotonously increase with increasing filter field strength (see [8] and [9]); the plasma confinement inside the driver is therefore a positive feature of the transverse FF downstream the driver region, when minimized inside the driver itself. Further analyses and measurements of the actual magnetic configuration were carried out, during SPIDER operation and shutdowns. From these results, it was clear that the PMs embedded in the lateral wall perturb the FF along the axis of the drivers, even at relatively high PG current (3kA), as shown in Fig. 10 of [10]. This is probably one of the underlying causes that contributed to the experienced left/right asymmetry of the source plasma properties: this effect was discussed in ref [11]. As reported, plasma light measurements of the left and right drivers show a discrepancy which depends on source parameters, the intensity of the FF and vertical position of the driver.

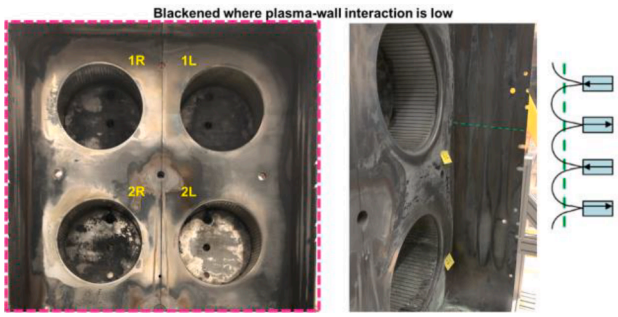

Fig. 2. Plasma driver plate, internal driver surfaces and lateral walls after the first 3.5 years of operation.

Furthermore, at the lateral wall, the sheath voltage is much higher than floating potential, i.e. almost no electron loss occurs. Therefore, it seems that the magnetic field at the wall (B_{wall}) is needlessly higher than necessary to ensure a low loss fraction. On the other hand, at the surfaces not protected by cusp magnets, during the present shutdown the disassembly of the source revealed rather clean surfaces indicating a certain level of plasma-wall interaction. This is the case of the drivers' exit on the plasma driver plate, as shown in Fig. 2 (left picture). During operation, a plasma density between 2×10^{17} m^{-3} with T_e of 4 eV, and 5×10^{17} m^{-3} with T_e of 10 eV, was measured at around the drivers' exit in an ad hoc campaign [12]. Considering the rather large area of such surface, a considerable plasma loss is associated with it. Instead, at surfaces already protected by cusp magnets such as each driver backplate and the SCLW, darker/dirtier areas were found, indicating to a certain degree a reduction of the plasma-wall interaction at those positions.

Therefore, the motivation for the proposed integration of new magnet sets into the source and the modification of some existing sets, described in detail in the following paragraphs, is threefold

- To reduce plasma losses at the source and driver walls in order to improve plasma density and generation efficiency;
- To reduce the interaction of the magnetic field produced by the SCLW on the FF, in order to eliminate the left-right non uniformity;
- To reduce the FF inside the driver to further improve the plasma confinement and generation efficiency.
- To achieve these three objectives three magnet systems were modified/integrated
- Rear Driver Plate (RDP): a new set of magnets in cusp configuration was added on the back wall of the expansion chamber to minimize the plasma losses there (see Fig. 10);
- SCLW: the original PM set was modified to minimize the interaction with the FF;

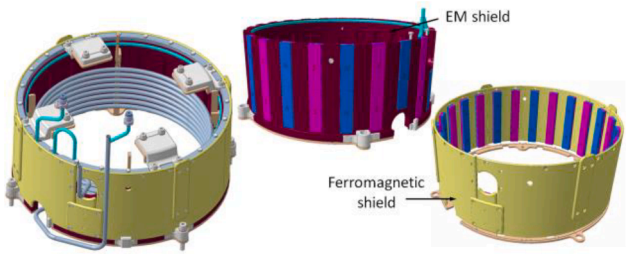

Fig. 3. Magnetic field norm along radial direction at φ=0° and different coordinate z.

- Around drivers: PMs are added to improve the plasma confinement and MSSs are introduced to concentrate their external flux and to minimize the FF inside the drivers.

2.1. Plasma losses estimation

The leak width w can be estimated as [13]

$$w \approx \frac{2}{\pi}(\rho_e \rho_i)^{0.5} \frac{d}{(\lambda_e \lambda_i)^{0.5}} \quad (1)$$

where ρ_e and ρ_i are the Larmor radii and λ_e and λ_i the mean free path of electrons and ions (generally different) respectively. This expression is valid for electro-positive plasmas, although the presence of negative ions in our application is expected to increase the leak width [14]. A figure of merit for the confinement efficiency is the loss fraction $f = w/d$, where d is the pitch among permanent magnets. In addition, the cusp field shields the region close to the wall in between the cusp magnets from plasma diffusion: this volume without plasma extends from the wall for a distance called Plasma Exclusion Zone (PEZ). A zero-order estimation of the losses at various source wall regions was carried out. The calculation of ion and electron currents are based on Bohm velocity and electron current for planar probe; plasma potential next to the surfaces, plasma density and electron temperature are derived for the various regions from measured parameters (derived from measurements with movable probes carried out in ad hoc campaign [9], but also integrated probes as already mentioned). The overall neutrality is imposed in the current balance, considering the areas of the various surfaces. The plasma grid PG, bias plate BP, lateral walls LW, source rear (plasma diver plate) are considered together with the surfaces of each driver, the Faraday shields of cylindrical shape and the driver backplate. The calculation shown that a large fraction of the plasma is lost at the Faraday shield (FS), i.e. the lateral surface of the drivers. For this reason, a great effort was devoted to integrating a new set of magnets in order to minimize the loss in the drivers, as described in the next paragraph.

3. New RF driver permanent magnets

In order to reduce the plasma losses inside the drivers and thus improve the plasma density and generation efficiency, a set of PMs around the driver was proposed. Different configurations were tested, considering the following requirements

- Maximized magnetic field at the FS inner wall;
- Minimized magnetic field outside the driver in order to prevent an increased electrical discharge probability;
- Uniform magnetic field along the driver circumference;
- Installation and disassembly of PM without removing SPIDER from vessel.

In particular, the second requirement imposes the use of MSS to channel the magnetic flux on the outer side of the driver inside the MSS

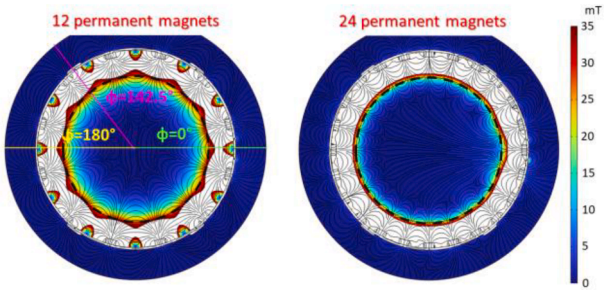

Fig. 4. Comparison between the 12 and 24 PMs driver configuration – contour plot on the midline cross section. FS position indicated by dashed black line.

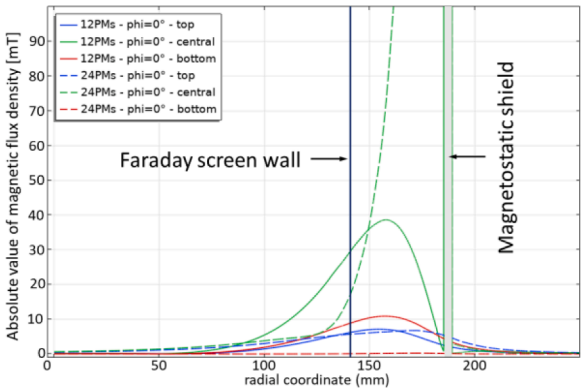

Fig. 5. Absolute value of the magnetic flux density along radial direction at φ=0° and different coordinate z, for the two configurations with 12 and 24 PMs.

itself. The presence of ferromagnetic material implies a change in the FF distribution, essentially in the driver region. This aspect is described in detail in Section 5. The limited space between two adjacent drivers and other pre-existing components around them, together with minimum PM dimensions in order to achieve a suitable magnetic field intensity and the presence of the MSS, implied a complete revision of the electromagnetic shield (EMS), including cooling circuit, RF coil support structure and part of the coil itself. In Fig. 3 the new design is shown: the complete assembly of RF coil, EMS and MSS is shown on the left, where the PMs are not visible; on the center-top of the figure only the EMS with the embedded PMs are shown; whereas at the bottom-right only MSS and PMs are shown.

The revised design includes

- Copper EMS, 12.25 mm thick with 24 cavities (2.25 mm min 4.1 mm max) to fit PMs with dimension 10 × 20 × 70 mm, in direct contact with the MSS;
- 24 or 12 SmCo PMs with nominal remanence B_r = 1.15 T (radial polarization, along 10 mm dimension);
- Ferromagnetic MSS 4 mm thick, made of 6 arcs for ease of assembly, with screwed parts for magnetic continuity and insulating blocks between EMS and source body.

3D finite element analysis, taking into account the non-linear BH dependence of the ferromagnetic material were carried out in the design phase. In the following, we will discuss the case with identical magnetization along each column of magnets, in the two options of 12 and 24 columns. The magnetic field produced by these cusp configurations is, neglecting edge effects, on the $r - \phi$ plane. An alternative configuration, not simulated here, is based on alternate magnetization along the magnet column, i.e. alternating polarization for all columns along the z coordinate (e.g. all S/N/S). In this configuration, the field lines of the

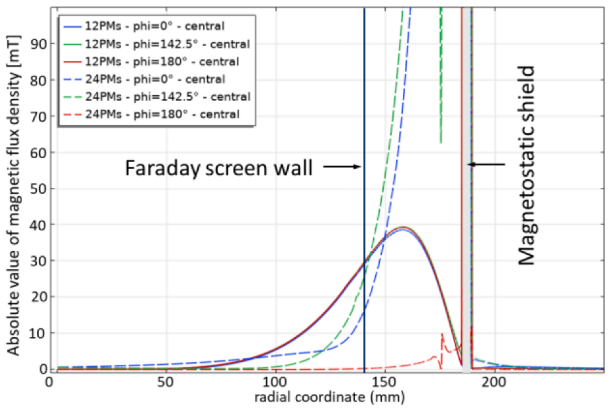

Fig. 6. Absolute value of the magnetic flux density along radial direction at driver midline cross section and different coordinate φ, for the two configurations with 12 and 24 PMs.

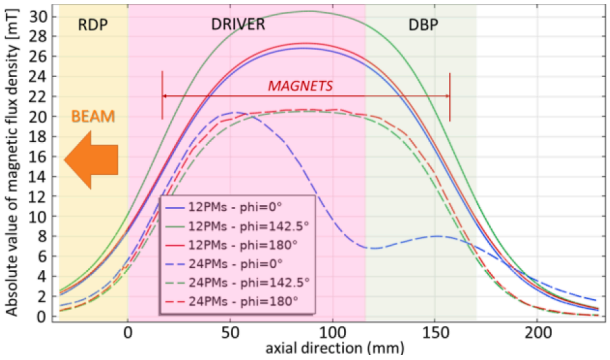

Fig. 7. Absolute value of the magnetic flux density along axial direction z and different coordinate φ, for the two configurations with 12 and 24 PMs. Driver Back Plate (DBP) is a stainless-steel disk closing the driver on the back side.

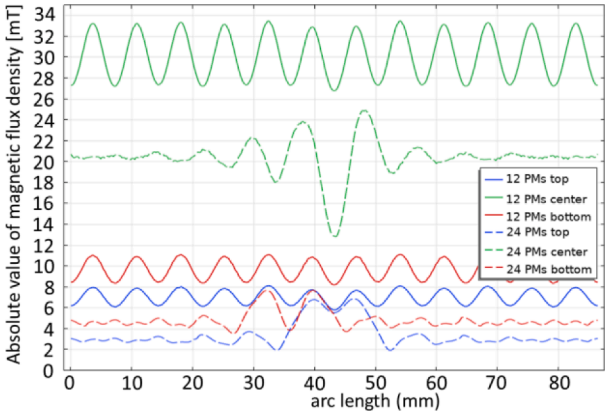

Fig. 8. Absolute value of the magnetic flux density along azimuthal direction φ and different coordinate z, for the two configurations with 12 and 24 PMs.

cusp magnets would lay on the $r-z$ plane. This alternative configuration, similar to ref. [15], could provide advantages for our design.

Fig. 4 shows the comparison between the magnetic field distribution across the midplane cross section of a single driver, produced by the new set of PMs only, in case 12 and 24 magnets are adopted. Contour regions where the field is higher than 35 mT are colored in white, value considered the optimal intensity at the FS wall.

In the following figures (Figs. 5–8) the absolute value of the magnetic flux density along relevant paths is shown.

Table 1
loss fraction and PEZ estimated for the two PM configurations foreseen in the driver cylindrical walls: the first number is calculated with Eq. (1), whereas the second one, pejorative, is extrapolated from preliminary PIC analyses.

PM #	B_0 [mT]	w [mm]	f [%]	PEZ (mm)
12	32	2.5–7	2.8–7.7	45–35
24	21	2–9	4.4–20	27–11

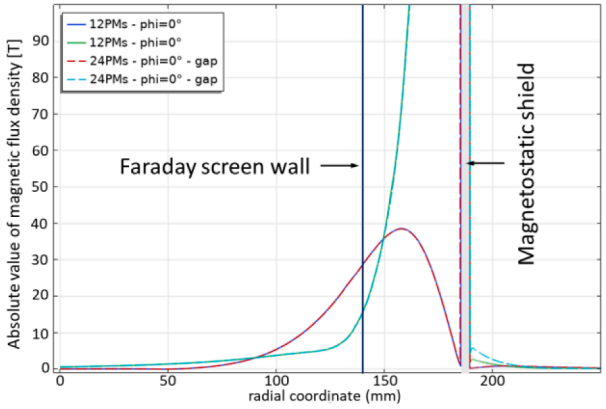

Fig. 9. Absolute value of the magnetic flux density along radial direction at driver midline cross section, for the two configurations with 12 and 24 PMs with and without 0.1 mm gap between MSS components.

In particular, the 24 PM configuration shows a more uniform field along the circumference, but it is more sensitive to discontinuities in the ferromagnetic shield and has a lower average intensity. Average magnetic field intensity and estimated loss fraction and PEZ for the two case are reported in Table 1.

Previous analyses consider a perfect contact between the MSS sectors and the ferromagnetic patches to assure the continuity of the magnetic circuit, which are screwed on the main sectors. The same analyses were repeated inserting a 0.1 mm gap between sectors and patches to test possible non-perfect contact on the field distribution. Fig. 9 is reported

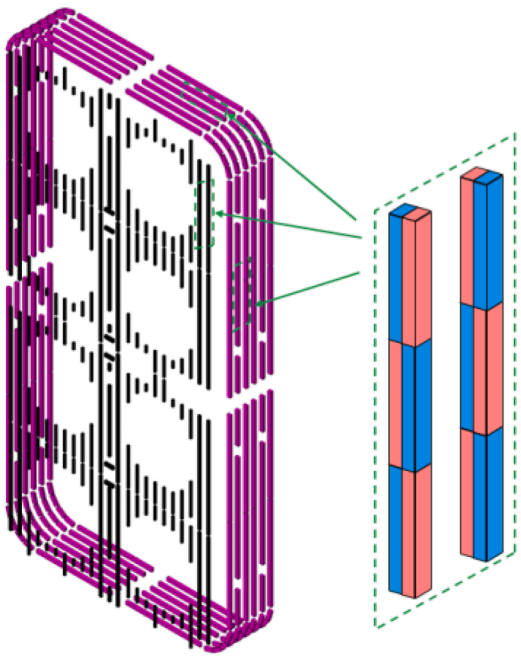

Fig. 10. New SCLW (purple) and RDP (gray) magnet sets; all PMs are arranged in a chessboard configuration.

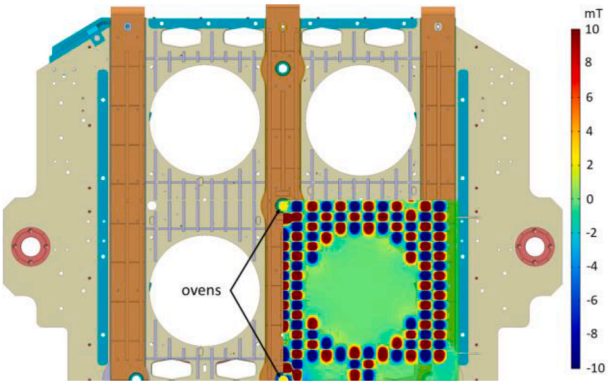

Fig. 11. CAD view of the top half of the RDP showing the magnet grooves, to which the contour plot of the normal component of the magnetic field is partially superimposed, showing the chessboard pattern.

to proof the negligible effect of the lack of magnetic continuity on the field distribution. In particular, only a slight increase of the field just outside the MSS is present in the case with gaps.

It is worth noting that the magnetic field due to the new PMs in the driver will of course affects the plasma generation. An increased plasma density is expected, but since only experimentation will be able to prove it, the design has been conceived in a modular fashion, allowing for permanent magnets and ferromagnetic material to be easily assembled and disassembled, in order to test different configurations by steps.

4. New configuration for lateral walls and rear driver plate

The original configuration included a set of PMs on the SCLW, arranged in four columns alternatively polarized, as described in [10]. This arrangement results in a plasma-wall interaction along the whole length of the magnets. The change to a chessboard configuration was proposed with a twofold purpose: on the one hand to further reduce the plasma-wall interaction to a smaller area at the center of each alternated magnet; on the other hand to cancel out on average the interaction between the magnetic field due to the magnets and the FF, as described in Section 5. Addition of PMs, again in chessboard arrangement, was proposed as well for the Rear Driver Plate (RDP), which is the back wall of the source case. The whole free space in between the drivers was used, taking into account the presence of previous constraints, such as diagnostic lines-of-sight and thermocouples. A 3D view of the SCLW (purple) and RDP (gray) magnet sets is shown in Fig. 10. A front CAD view of the top half of the RDP with the magnet grooves, to which the contour plot of the normal component of the magnetic field is partially superimposed to highlight the chessboard pattern, is shown in Fig. 11.

The number of columns of SCLW PMs was increased to six, at a shorter distance from each other and with PMs of smaller dimensions. As a matter of fact, the intensity of the magnetic field of the original set at the SCLW was measured to be between 110 and 120 mT and considered excessive. Magnets on the corners were added, following the same change in polarization as the lateral ones. Concerning the RDP magnets, some of them are embedded on the steel plate that constitutes the actual RDP, whereas others on the bus bars which carry the PG current producing the FF. Dimensions and distances of the magnets were optimized, considering the two sets simultaneously, in order to preserve symmetries around the drivers and between the source case walls, and taking into account preexisting geometrical constrains. SmCo was chosen for all PMs, for their quite high remanence and excellent thermal behavior up to 250 °C. In particular the following sets are foreseen

- PMs of 9 × 13 × 25 mm and nominal remanence of 0.94 T (polarization along 13 mm dimension) on the SCLW;

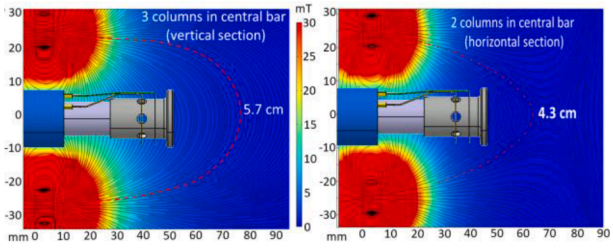

Fig. 12. Comparison between the magnetic field produced around the Cs oven tip by the two PM configurations considered: with three PM columns and dedicated PMs on the central bus-bar (left, vertical cross section), with two PM columns on the central bus-bar (right, horizontal cross section).

- PMs of 9 × 13 × 35 mm and nominal remanence of 0.94 T (polarization along 13 mm dimension) on the SCLW corners;
- PMs of 7 × 7 × 25 mm and nominal remanence of 0.94 T (polarization along 7 mm dimension) on the RDP;
- PMs of 7 × 9 × 25 mm and nominal remanence of 1.15 T (polarization along 7 mm dimension) on the PG bus bars.

The optimization of the magnetic field produced by the RDP magnets was carried out taking into account also the presence of the cesium ovens. Indeed, the localized magnetic field produced by the new PMs, whether suitably arranged, can be exploited to protect the oven tip against the plasma. Two configurations were considered in this respect: one with only two columns of PMS embedded in the central PC current bus-bar, exploiting the magnetic field produced by themselves on the horizontal plane as magnetic mirror; the other with three columns of PMs and a pair of additional PMs above and below each of the three ovens, producing a magnetic field on the vertical plane. Advantage of the first choice would be to have the same number of PMs on the central and lateral bus-bars, thus facilitating the PG current distribution, and not to break locally the symmetry of the magnetic distribution due to the RDP magnets. Advantage of the second one is to maintain the same pace between neighboring PM columns, to maintain an overall left-right symmetry (which makes the right combination between RDP and lateral SCLW magnets on both left and right sides) and finally, by adopting ad hoc PMs, the magnetic field in front of the oven is higher and consequently the field lines are longer (larger PEZ), as shown in Fig. 12.

Estimation of the loss fraction for the final configuration, taking into account Eq. (1), gives $f \approx 2.5\%$. It is worth noting that the latter is an underestimation of the actual loss fraction, since it does not take into account the presence of negative ions and it is not validated for checkerboard configuration. However, it provides a good motivation for adopting the proposed configuration.

It is worth nothing that in principle the loss fraction on the lateral walls has probably increased compared to the old configuration (both the distance between the magnets and the field strength have been reduced), but the main goal of the adopted design is the reduction of the interaction of SCLW PMs magnetic field with the FF.

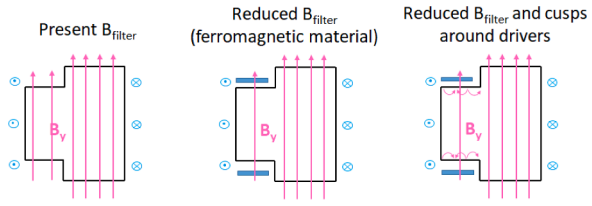

Fig. 13. Simplified schematics of the three testing conditions for the upgraded driver magnetic configurations.

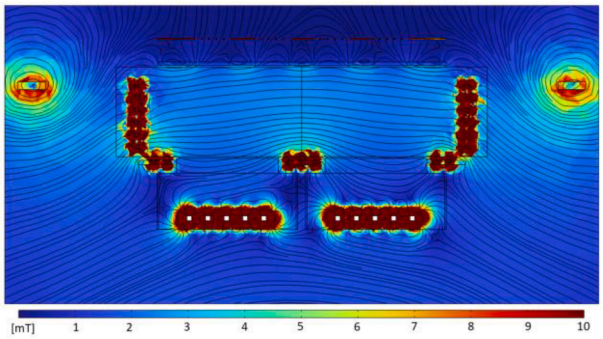

Fig. 14. Magnetic field distribution (on the midplane cross section of central drivers) without the ferromagnetic shield around the drivers, at 1.5 kA PG current.

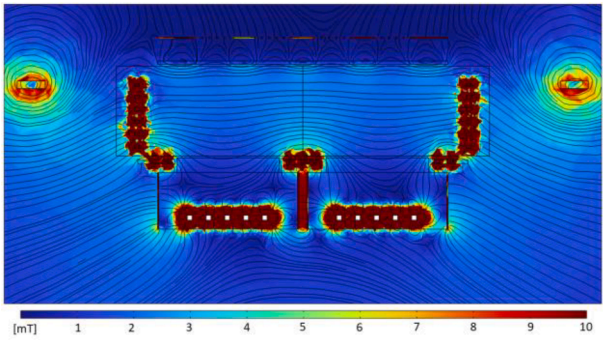

Fig. 15. Magnetic field distribution (on the midplane cross section of central drivers) with the ferromagnetic shield around the drivers, at 1.5 kA PG current.

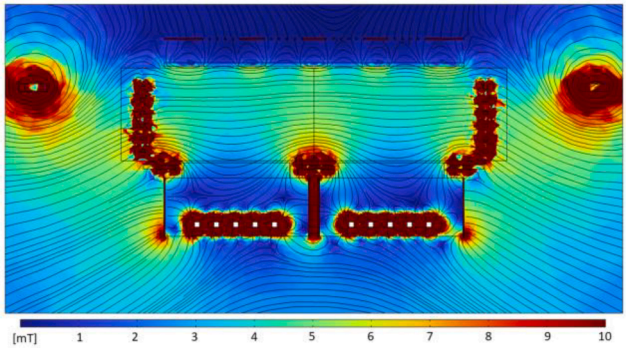

Fig. 16. Magnetic field distribution (on the midplane cross section of central drivers) with the ferromagnetic shield around the drivers, at 3 kA PG current.

5. Overall magnetic field

The modification of the FF configuration described in [8] improved the plasma generation in the driver [16–18], which however is still affected by the FF intensity [10]. The addition of magnets and MSS around the drivers allows testing three different conditions regarding the FF in the drivers, as sketched in Fig. 13, that is

- Pre shut-down condition, without MSS nor PMs;
- Addition of MSS only should reduce the FF inside the driver, thus changing plasma confinement properties related to the plasma bulk and not to its boundary;
- MSS and PMs: in addition to the reduction of FF due to the ferromagnetic shield, the plasma boundary is also improved.

3D FEM analyses, similar to those described in [10], were carried out in order to verify the new configuration as a whole. Specifically, the 3D model takes into account all the magnetic field sources (PG current, permanent magnets and ferromagnetic material on the Grounded Grid and drivers), except the PMs on the drivers, whose contribution was studied in detail in the dedicated analyses described in Section 3. Compared to the results presented in [10], Fig. 14, which reports the magnetic field distribution without the ferromagnetic shield around the drivers for 1.5 kA PG current, shows that choosing the chessboard arrangement for the SCLW PMs cancels the left-right asymmetry of the overall magnetic field distribution inside the source case, as expected.

The presence of the ferromagnetic structure around each driver (even though discontinuous) reduces the transverse field inside the drivers due to PG current, as shown in Figs. 15 and 16, in particular from 3.5mT to 1.5mT at the center for 3kA PG current.

The driver MSSs contribute also to make more symmetric the field distribution inside the drivers and to make it more uniform in front of the PG. The only possible disadvantage one can conceive of at the moment is the intensified magnetic field between pairs of drivers horizontally and at the side back ends, which reaches 20 mT and peaks of 30 mT respectively. This could increase the breakdown probability, which is difficult to predict in advance. Hence a step-by-step strategy is foreseen at the restart of SPIDER, testing first the new configuration without both PMs and MSS on the driver, then adding the MSS and eventually the PMs, with the possibility to test both the configuration with 12 and 24 PMs per driver.

6. Conclusions

Taking advantage of the long SPIDER shut-down started at the end of 2021, for necessary maintenance and planned refurbishments, modification and addition of sets of permanent magnets in the plasma source expansion chamber and around the RF driver was studied and proposed. The new configuration aims on the one hand at improving plasma generation efficiency and maximizing plasma density, and on the other hand at reducing the residual left-right asymmetry.

Declaration of Competing Interest

The authors declare that they have no known competing financial interests or personal relationships that could have appeared to influence the work reported in this paper.

Data availability

Data will be made available on request.

Acknowledgments

This work has been carried out within the framework of the ITER-RFX Neutral Beam Testing Facility (NBTF) Agreement and has received funding from the ITER Organization. The views and opinions expressed herein do not necessarily reflect those of the ITER Organization.

References

[1] D. Campbell, Preface to special topic: ITER, Phys Plasmas 22 (2015), 021701, https://doi.org/10.1063/1.4906215.
[2] T Inoue, et al., Fus. Eng. Des. 517 (2001) 56–57.
[3] V. Toigo, et al., New J. Phys. 19 (2017), 085004.
[4] G. Serianni, et al., SPIDER in the roadmap of the ITER neutral beams, Fus. Eng. Des. 146-B (2019) 2539–2546, https://doi.org/10.1016/j.fusengdes.2019.04.036.
[5] M.A. Lieberman, A.J. Lichtenberg, Principles of Plasma Discharges and Material Processing, John Wiley and Sons, New Jersey, 2005.
[6] Y. Takeiri, Negative ion source development for fusion application, Rev. Sci. Instrum. 81 (2010) 02B114, https://doi.org/10.1063/1.3274806.

[7] N. Marconato, et al., Simulation, code benchmarking and optimization of the magnetic field configuration in a Negative Ion Accelerator, Fus. Eng. Des. 86 (2011) 925–928, https://doi.org/10.1016/j.fusengdes.2011.01.052.
[8] N. Marconato, et al., An optimized and flexible configuration for the magnetic filter in the SPIDER experiment, Fus. Eng. Des. 166 (2021), 112281, https://doi.org/10.1016/j.fusengdes.2021.112281.
[9] E. Sartori, et al., Development of a set of movable electrostatic probes to characterize the plasma in the ITER neutral beam negative-ion source prototype, Fus. Eng. Des. 169 (2021), 112424, https://doi.org/10.1016/j.fusengdes.2021.112424.
[10] N. Marconato, E. Sartori, G. Serianni, Numerical and experimental assessment of the new magnetic field configuration in SPIDER, IEEE Transact. Plasma Sci. (2023), https://doi.org/10.1109/TPS.2022.3167859.
[11] G. Serianni, et al., SPIDER, the negative ion source prototype for ITER: overview of operations and caesium injection", accepted for publication, in: In IEEE Transactions on Plasma Science, 2023.
[12] V. Candeloro, et al., Development of a triple langmuir probe for plasma characterization in SPIDER, in: IEEE Transactions on Plasma Science, 2022, https://doi.org/10.1109/TPS.2022.3173885.
[13] C. Koch, G. Matthieussent, Phys. Fluids 26 (1983) 545.
[14] V. Candeloro, et al., Influence of plasma parameters on the effectiveness of multi-cusp magnetic field confinement in negative ion source, J. Instrument. (2023).
[15] C.S. Ren, D.Z. Wang, J. Zhang, X.L. Qi, Y.N. Wang, The effect of external cusp magnetic field on Ar ICP characteristics, Vacuum 83-2 (2008) 423–426, https://doi.org/10.1016/j.vacuum.2008.04.074.
[16] V. Toigo, et al., On the road to ITER NBIs: SPIDER improvement after first operation and MITICA construction progress, Fusion Eng. Des 168 (2021), 112622, https://doi.org/10.1016/j.fusengdes.2021.112622.
[17] A. Pimazzoni, et al., Co-extracted electrons and beam inhomogeneity in the large negative ion source SPIDER, Fus. Eng. Des. 168 (2021), 112440, https://doi.org/10.1016/j.fusengdes.2021.112440.
[18] E. Sartori, et al., Nucl. Fusion 62 (2022), 086022.